EDGE TURBULENCE MEASUREMENTS IN TFTR

S.J. ZWEBEN, D. MANOS, R.V. BUDNY, P. EFTHIMION, E. FREDRICKSON,
H. GREENSIDE, K.W. HILL, S. HIROE *, S. KILPATRICK, K. McGUIRE, S.S. MEDLEY,
H.K. PARK, A.T. RAMSEY and J. WILGEN *

Princeton Plasma Physics Laboratory, Princeton, NJ 08544, USA

The edge turbulence in TFTR is characterized by several diagnostics. Langmuir probes and D-alpha imaging have detected large amplitude, small-scale, broadband density fluctuations in the scrape-off region near the wall. Broadband fluctuations with a similar frequency spectrum are detected by small-angle microwave scattering and magnetic pickup loops. Increases in the turbulence level are seen during neutral beam injection. Some preliminary analysis of this data is presented.

1. Introduction

Several measurements of edge turbulence have been made in TFTR during the recent run period, which included discharges with up to 13 MW of neutral beam injection. Although this turbulence data set is not yet complete, some representative trends are described and a preliminary analysis and interpretation is given.

For the purposes of this paper, the term "edge" refers mainly to the region between the last closed flux surface and the wall (the "scrape-off layer"), but also in some cases to the peripheral region of the main plasma at roughly $r/a > 0.7$ and $T_e < 1$ keV. "Turbulence" here means incoherent fluctuations in plasma density, potential, or magnetic field which are typically strongest in the frequency range 10–1000 kHz and spatial scale range 0.1–10 cm. Previous measurements in tokamaks have shown that similar turbulence exists on either side of the last closed flux surface, i.e. in both these parts of the "edge" [1].

From the viewpoint of plasma–surface interactions, the edge region is important in that it determines the heat and particle fluxes to the limiters, walls, or divertor plates. From the viewpoint of plasma confinement physics, the edge region is significant since it apparently affects global plasma confinement [2,3], as in the L–H transition. In either case it is clearly useful to understand the mechanisms which govern the edge cross-field heat conduction and particle diffusion.

Several measurements in small tokamaks [4–10] have already shown that the outward particle flux due to the turbulent density fluctuations $\tilde{n}$ and their associated $E \times B$ drifts are largely responsible for the usual "Bohm" diffusion observed in the scrape-off region [11]. The heat flux in this region also appears to be dominated by the large turbulent n [9,10,12]. However, it remains to be seen whether the n or possibly the

---

* Oak Ridge National Laboratory, Oak Ridge, TN 37830, USA.

magnetic $\tilde{B}$ turbulence is dominant in the higher temperature regions in the edge of TFTR plasmas.

In section 2–5 are descriptions of the edge turbulence measurements which are currently available on TFTR, in section 6 is an analysis of the fractal dimensionality of some of this data, and in section 7 is a brief summary.

2. Langmuir probe measurements

Langmuir probes have been used in several small tokamaks to study edge turbulence [1]. In TFTR the Langmuir probes are made of robust 0.5 cm diameter graphite rods; even so, the high heat fluxes in the edge region generally restrict their use to the scrape-off region outside the last closed flux surface [13].

Some data obtained from a radial scan of three closely spaced Langmuir probes is shown in fig. 1(a) for ohmic discharges with relatively low current (0.5 MA) and low density ($n = 2 \times 10^{13}$ cm^{-3}). These discharges were bounded at the outer movable limiter, and the probe was scanned 4–13 cm outside the last closed flux surface, just below the outer equatorial plane. Density and temperature inferred from the double probe characteristics are shown in this figure, along with $\tilde{n}/n$ and $\tilde{\phi}/T_e$ obtained from the saturation current and floating potential of the third probe in the usual way [4].

Broadband turbulent fluctuations were observed with these probes in the frequency range 10–200 kHz, with typical fluctuation levels of $\tilde{n}/n = 0.3$–0.5 and $\tilde{\phi}/kT_e = 0.1$. These results are roughly consistent with those obtained in the scrape-off layers of smaller tokamaks [4,5].

The effect of 5 MW of neutral beam injection on the spectrum of floating potential fluctuations is shown in fig. 1(b) for a probe 10 cm behind the last closed flux surface. The spectrum shifts to higher frequencies with injection, and the amplitude of $\tilde{\phi}$ increases from 2 to 9 volts rms with injection. These changes are most likely associated with the local effects of injection on the edge plasma parameters [14].
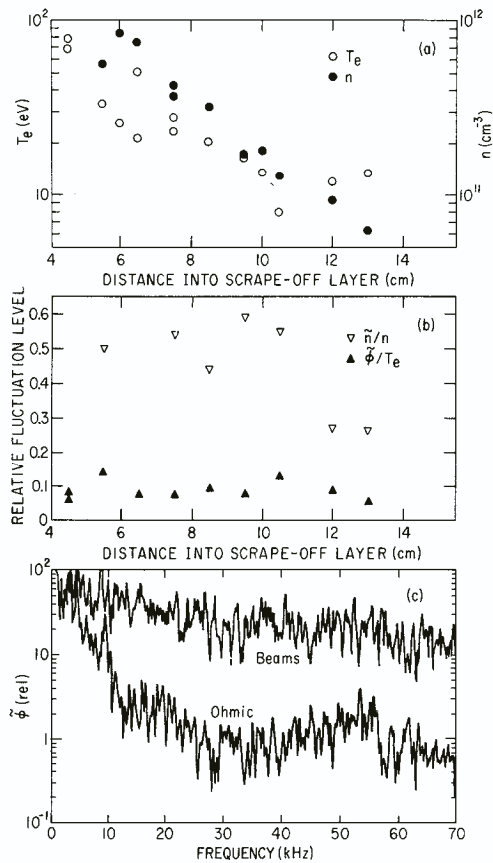
Fig. 1. Results from a radial scan of Langmuir probes in the scrape-off region of an ohmic TFTR discharge. In (a) and (b) are the average densities, temperatures and relative fluctuation levels in this region, and in (c) are frequency spectra of the floating potential with and without neutral beam injection.

3. D-alpha imaging

Visible imaging of the light emitted by tokamaks has already been used to diagnose edge turbulence [15–17]. The results reported here used a gated, intensified video camera to view the D-alpha emission from the inner limiter region of TFTR. Note that the intensity of D-alpha emission is proportional to the local electron density times the local neutral density, so that the light emission follows the fluctuating electron density (while the neutral density most likely does not fluctuate on these timescales).

In fig. 2 is an image of D-alpha radiation from a region ≈ 100 cm square on the inner toroidal-shaped bumper limiter, taken with an exposure time of ≈ 10 μs. This view is centered about 30° above the midplane, with the "filaments" in the D-alpha emitting annulus lying just above the inner limiter (the plasma center is

Fig. 2. Image of D-alpha light at the inner limiter scrape-off region taken with an exposure time of ≈ 10 μs. The bright stripes are filaments of D-alpha which are elongated approximately along the magnetic field lines. The apparent toroidal variation is due to modulation of the neutral density along the inner wall, and not to $\tilde{n}$. These "filaments" fluctuate in position from frame-to-frame, but have a poloidal spacing of typically 5–10 cm.

toward the lower right out of this field of view).

These filaments of D-alpha emission are aligned approximately along the direction of the local magnetic field, and are spaced irregularly in the poloidal direction. Their positions vary irregularly from frame-to-frame, i.e. their temporal correlation is much less than the time between frames of 16 ms. Very similar observations were made in diverted ohmic ASDEX discharges [15]. We interpret these filaments as due to the edge $\tilde{n}$ perturbations, which are known to be elongated toroidally with relatively short correlation lengths poloidally.

The clearest filaments such as shown in fig. 2 were observed during neutral beam injection. Similar but less clearly defined filaments were seen during the ohmic phases of the same discharge. Based on the interpretation above, we can characterize the edge turbulence in this region as having wavelengths in the range 5–10 cm over the frequency range $f < 50$ kHz (half-period less than 10 μs), with typical amplitudes $\tilde{n}/n > 20\%$ during injection. The radial location of these filaments is difficult to specify precisely. However, since the D-alpha

region is of thickness 3–5 cm, and since the scrape-off thickness in this region is about 3 cm, it is likely that the filaments shown in fig. 2 are located in the scrape-off region where $T_e = 5$–50 eV.

It is interesting to note that a wider-angle view of the entire inner limiter surface in D-alpha emission in the same discharges shows no clear filamentary structures in the wavelength range 20–100 cm, except for those associated with coherent MHD during plasma startup and MARFES. Thus there does not appear to be any large-scale turbulence under normal conditions.

4. Far-forward microwave scattering

Electron density fluctuations were also monitored by observing the frequency-shifted components of the 1
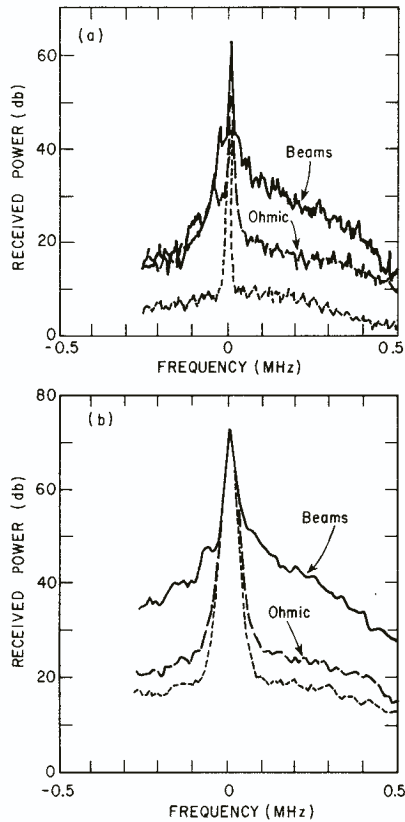

Fig. 3. Spectra of the transmitted microwave signal showing sidebands due to scattering from density fluctuations. In (a) are the spectra from the ohmic and neutral beam phases of a normal TFTR discharge, which show the increased scattering during beams, a trend which is seen even more clearly in the "energetic ion mode" discharge shown in (b). The bottom trace in each figure is the signal with no plasma present. These spectra are asymmetric in frequency due to a slight misalignment of the interferometer system.

mm microwave interferometer (which is normally used for line-averaged density measurements). These frequency shifts or sidebands of the transmitted microwave signal are due to small-angle forward scattering by density fluctuations $\tilde{n}$; in this geometry the scattering occurs predominantly in the outer edge region near the recieving horn in the wavenumber range $\lambda_{pol} > 2$–3 cm. The transmitted signal is monitored using a swept spectrum analyzer in the frequency range ± 500 kHz around the unshifted center frequency. The scattered power at any non-zero frequency is proportional to $\tilde{n}^2$.

In fig. 3(a) are typical spectra for the ohmic and neutral beam injected phases of a single TFTR discharge with $I = 2.2$ MA, $n = 5 \times 10^{13}$ cm^{-3}, $B = 4.8$ T, and $P_{beam} = 10$ MW. In the ohmic phase the scattered power is above the synchrotron background only in the frequency range -100–0 kHz; however, during neutral beam injection the scattered power rises significantly above the ohmic level over the range -100 kHz $< f <$ 500 kHz.

In fig. 3(b) is a spectrum taken during the ohmic and beam phases of a discharge in the "energetic ion mode", here with $I = 0.7$ MA, $n = 2 \times 10^{13}$ cm^{-3}, $B = 4$ T, and $P_{beam} = 9$ MW. This regime is characterized by a relatively high ion temperature and a relatively low global energy confinement time. The scattered power in this case increased by at least $\times 4$ relative to the discharge in 3(a), while the spectrum is roughly the same, i.e. $P(f) \propto f^{-1.5 \pm 0.5}$ over 100 kHz $< f <$ 300 kHz.

The characteristics of these fluctuations are at least qualitatively similar to those seen in previous scattering measurements on tokamaks with neutral beam injection [1]. In those cases and here the increased scattering with increased beam power suggested a correlation between increased turbulence and decreased confinement; however, the connection remains to be quantified.

5. Magnetic pickup loops

Magnetic pickup loops (Mirnov coils) located inside the TFTR vacuum vessel but well outside the plasma have been used to study magnetic fluctuations. The coils are located inside the vessel wall such that the coil nearest the plasma is 11 cm from the last closed flux surface. The coil signals are digitized at 500 kHz for the data presented here. At $f < 250$ KHz these probes respond to dB_θ/dt.

Broadband fluctuations have been observed in both ohmic and neutral beam heated discharges. Typical $\tilde{B}_\theta$ spectra are shown in fig. 4, where for this case the coil closest to the plasma at the inner equatorial plane is used. The frequency spectra are of the form $\tilde{B}_\theta \propto f^{-1.0 \pm 0.5}$ for both ohmic and beam cases; however, the fluctuation amplitude increases substantially with beam power, up to $|\tilde{B}_\theta|/B_\varphi = 2 \times 10^{-5}$ at the highest beam powers for the innermost coil. Comparisons of the fluctuation level measured by coils at different distances
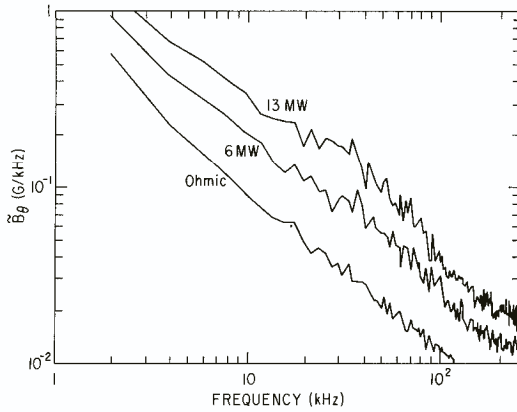
Fig. 4. Spectra of $\tilde{B}_\theta$ seen by a coil 11 cm from the plasma edge at the inner equatorial plane. The magnitude of the braodband fluctuations increases during neutral beam injection.

from the plasma edge, corresponding to different poloidal angles, show that there is an approximately exponential fall-off of $\tilde{B}_\theta$ amplitude over about 5 cm in the scrape-off layer. This, along with the lack of correlation between coils separated by 30 cm poloidally, suggests that the turbulence is composed of modes with high m (i.e. $m > 15$). Note that the D-alpha filament wavelength of 5–10 cm poloidally corresponds to an $m \approx 50$–100.

The correlation between increased broadband $\tilde{B}_\theta$ amplitude and decreased confinement with neutral beam heating has been observed previously [1]. However, from measured $|\tilde{B}_\theta|$ at the wall it is not possible to quantify the transport effects inside the plasma.

6. Fractal dimensionality

Recent advances in the the theory of dynamical systems suggest novel ways to analyze the time series obtained by various probes of edge turbulence [18]. These advances suggest that these time series, when embedded into some higher dimensional space, should form a fractal object with certain scaling properties. The exponents of these scaling relations estimate the complexity of the turbulence, in the sense that they approximate the minimum number of degrees of freedom (coupled ordinary differential equations) whose dynamics could generate such a time series.

This approach makes the fundamental assumption that the observed broadband spectra derive from nonlinear interactions of only a few degrees of freedom. This is contrary to the traditional assumption that turbulence consists of infinitely many degrees of freedom, each corresponding to an independent oscillator.

Applications of these ideas to edge turbulence obtained on DITE [19] recently suggested the unexpected
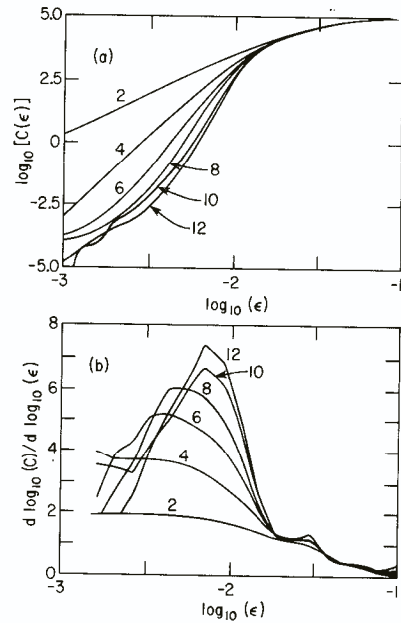

Fig. 5. Analysis of the fractal dimensionality of the floating potential fluctuations of the Langmuir probe data similar to that shown in fig. 1. The correlation integral $C(\epsilon)$ is calculated for different ball sizes ϵ for six embedding dimensions (2, 4, 6, 8, 10, 12) using time series of 8192 points [18]. In (a) $\log_{10}C(\epsilon)$ is plotted verses $\log_{10}(\epsilon)$; scaling occurs when this curve is linear. In (b) the derivative of splines that have been least-squares fitted gives the local slope (fractal dimensionality). The steady increase of dimensionality with increasing embedding dimension suggests that the data is not well approximated by a few degrees of freedom.

result that edge turbulence can be quite simple, having as few as 2 and 3 degrees of freedom. We have repeated this analysis on recent floating potential probe data described above.

Our results (see fig. 5) suggest that there are small regimes of scaling around one and below one but no consistent scaling at higher dimensions. These results are independent of several details of the algorithm, such as the embedding dimension and the time delay used for embedding.

We draw several conclusions. First, the traditional plot for extracting the scaling (correlation) exponent can be misleading. Although a log–log plot as in fig. 5(a) shows large regions of seemingly linear behavior (scaling), an examination of the slope shows that the derivative is constantly varying except in several small regions, where a scaling exponent near one is observed, as shown in fig. 5(b). (This low exponent may be a simple periodic mode present in the turbulence.) This more careful analysis should also be applied to the data already quoted in the literature.

Second, our plots are inconsistent with a scaling that suggests a low dimensional dynamical system. The plateaus above one increase with embedding dimension, which is characteristic of high-dimensional systems or white noise. Further studies are currently being carried out to extend this analysis to other types of TFTR data, and to explore possible radial dependences of the dimensionality.

7. Summary

Taken together, the measurements described in sections 2–5 show that the edge turbulence in TFTR is similar to that seen in smaller tokamaks, the main features being:

(a) strong density turbulence in the scrape-off region, with $\tilde{n}/n \approx 0.3$–0.5,

(b) weak magnetic turbulence, with $\tilde{B}_\theta/B_\varphi \approx 2 \times 10^{-5}$ at the wall,

(c) broadband spectra of $\tilde{n}$, $\tilde{\phi}$, and $\tilde{B}$ in the frequency range 10–1000 kHz, with approximate power-law dependences $P(f) \propto f^{-1.0 \pm 0.5}$,

(d) short poloidal wavelengths of $\tilde{n}$ and $\tilde{B}_\theta$, in the range corresponding to "mode numbers" $m > 15$, i.e. small-scale compared with the plasma size, and

(e) increased amplitude of $\tilde{n}$ and $\tilde{B}_\theta$ fluctuations with neutral beam injection.

There is not yet enough information available to understand either the transport effects or the underlying physical processes of this turbulence. Further measurements will aim to calculate directly the $\tilde{E} \times B$ induced transport in the scrape-off layer, to measure the radial structure of the magnetic turbulence, and to correlate more precisely the fluctuation strengths with local edge gradients and with global transport.

References

[1] P.C. Liewer, Nucl. Fusion 25 (1985) 543.
[2] H.P. Furth, Plasma Phys. and Contr. Fusion 28 (1986) 1305.
[3] B.B. Kadomtsev, Comm. Plasma Phys. and Cont. Fusion 9 (1985) 227.
[4] S.J. Zweben and R.W. Gould, Nucl. Fusion 25 (1985) 171.
[5] S.J. Levinson et al., Nucl. Fusion 24 (1984) 527.
[6] C.P. Ritz et al., Phys. Fluids 27 (1984) 2954.
[7] V.P. Budaev and R.S. Ivanov, Seventh European Conf. on Plasma Physics, Budapest (1985), paper AP FR 024.
[8] R.L. Hickok et al., Seventh European Conf. on Plasma Physics, Budapest (1985), paper AP FR 012.
[9] A. Howling et al., Seventh European Conf. on Plasma Physics, Budapest (1985), paper AP FR 026.
[10] A.J. Wootton et al., Oak Ridge Report ORNL-TM-9305 (1986).
[11] S.J. Zweben and R.J. Taylor, Nucl. Fusion 23 (1983) 513.
[12] P.C. Liewer et al., Phys. Fluids 29 (1986) 309.
[13] S.J. Kilpatrick et al., Princeton Univ. Report PPPL-2284 (1986).
[14] R. Budny et al., these Proc. (PSI-VII), J. Nucl. Mater. 145–147 (1987).
[15] D.H.J. Goodall, J. Nucl. Mater. 111 & 112 (1982) 11.
[16] S.J. Zweben et al., Nucl. Fusion 23 (1983) 825.
[17] K. Yamazaki et al., J. Nucl. Mater. 128 & 129 (1984) 186.
[18] P. Grassberger and I. Procaccia, Physica 9D (1983) 189.
[19] W. Arter and D.N. Edwards, Phys. Lett. 114A (1986) 84.